

Independently Evolved Virulence Effectors Converge onto Hubs in a Plant Immune System Network

M. Shahid Mukhtar,^{1*†} Anne-Ruxandra Carvunis,^{2,3,4*} Matija Dreze,^{2,3,5*} Petra Epple,^{1*} Jens Steinbrenner,⁶ Jonathan Moore,⁷ Murat Tasan,⁸ Mary Galli,⁹ Tong Hao,^{2,3} Marc T. Nishimura,¹ Samuel J. Pevzner,^{2,3,10,11} Susan E. Donovan,^{6‡} Lila Ghamsari,^{2,3} Balaji Santhanam,^{2,3} Viviana Romero,^{2,3} Matthew M. Poulin,^{2,3} Fana Gebreab,^{2,3} Bryan J. Gutierrez,^{2,3} Stanley Tam,^{2,3} Dario Monachello,¹² Mike Boxem,¹³ Christopher J. Harbort,^{1§} Nathan McDonald,¹ Lantian Gai,⁹ Huaming Chen,⁹ Yijian He,¹ European Union Effectoromics Consortium, Jean Vandenhoute,⁵ Frederick P. Roth,^{2,14¶} David E. Hill,^{2,3} Joseph R. Ecker,^{9,15} Marc Vidal,^{2,3¶¶} Jim Beynon,^{6,7¶¶} Pascal Braun,^{2,3¶¶} Jeffery L. Dangl^{1,16,17,18¶¶}

Plants generate effective responses to infection by recognizing both conserved and variable pathogen-encoded molecules. Pathogens deploy virulence effector proteins into host cells, where they interact physically with host proteins to modulate defense. We generated an interaction network of plant-pathogen effectors from two pathogens spanning the eukaryote-eubacteria divergence, three classes of *Arabidopsis* immune system proteins, and ~8000 other *Arabidopsis* proteins. We noted convergence of effectors onto highly interconnected host proteins and indirect, rather than direct, connections between effectors and plant immune receptors. We demonstrated plant immune system functions for 15 of 17 tested host proteins that interact with effectors from both pathogens. Thus, pathogens from different kingdoms deploy independently evolved virulence proteins that interact with a limited set of highly connected cellular hubs to facilitate their diverse life-cycle strategies.

Interactions between disease-causing microbes and their hosts are complex and dynamic. Plants recognize pathogens through two major classes of receptors. Initially, plants sense microbes via perception of conserved microbe-associated molecular patterns (MAMPs) by pattern-recognition receptors (PRRs) located on the cell surface. This first level of recognition results in MAMP-triggered immunity (MTI), which is sufficient to fend off most microbes (1). To counter MTI, evolutionarily diverse plant pathogens independently evolved mechanisms to secrete and deliver effector proteins into host cells (2, 3). Effectors interact with cellular host targets and modulate MTI and/or host metabolism in a manner conducive to pathogen proliferation and dispersal (3–5). Plants deploy a second set of polymorphic intracellular immune receptors to recognize specific effectors. Nearly all are members of the nucleotide-binding site–leucine-rich repeat (NB-LRR) protein family, analogous to animal innate immune NLR proteins (6, 7). NB-LRR proteins can be activated upon direct recognition of an effector or indirectly by the action of an effector protein on a specific host target (3–5). NB-LRR activation causes effector-triggered immunity (ETI), which is essentially a high-amplitude MTI response that results in robust disease-resistance responses that often include localized host cell death and systemic defense signaling (3, 5).

We systematically mapped physical interactions between proteins from the reference

plant *Arabidopsis thaliana* (hereafter, *Arabidopsis*) and effector proteins from two pathogens: the Gram-negative bacterium *Pseudomonas syringae* (*Psy*) and the obligate biotrophic oomycete *Hyaloperonospora arabidopsidis* (*Hpa*). These two pathogens last shared a common ancestor over 2 billion years ago and use vastly different mechanisms to colonize plants. Despite independent evolution of virulence mechanisms, we hypothesized that these two pathogens would deploy effectors to manipulate a largely overlapping set of core cellular MTI machinery (4, 5).

Mapping of a plant-pathogen protein-protein interactome network. We used experimentally validated *Psy* effector proteins (8), candidate effectors from *Hpa* (9, 10), and immune-related *Arabidopsis* proteins or “immune proteins” including the following: (i) N-terminal domains of NB-LRR intracellular immune receptors; (ii) cytoplasmic domains of LRR-containing receptor-like kinases (RLKs), a subclass of PRRs; and (iii) known signaling components or targets of pathogen effectors (defense proteins) (fig. S1 and table S1) (10). We mapped binary protein-protein interactions between these 552 immune and pathogen proteins and the ~8000 full-length *Arabidopsis* proteins (AtORFeome2.0) used to generate the *Arabidopsis* interactome, version 1 (AI-1), using the same yeast two hybrid–based pipeline (10–12). This resulted in an experimentally determined plant-pathogen immune network containing 1358 interactions among 926 proteins, including 83 pathogen effectors, 170 immune proteins, and

673 other *Arabidopsis* proteins (hereafter, immune interactors) (Fig. 1A and table S2) (10). Because our data set was acquired using the same pipeline as that used to define AI-1 (11), we estimate that the two data sets are equivalent in quality with (i) a coverage of ~16% of all possible interactions within the tested space (fig. S1) and (ii) a proportion of true biophysical interactions statistically indistinguishable from that of well-documented high-quality pairs from the literature (11). We combined our data set with interactions from AI-1 and literature-curated interactions (LCI) (11) involving the same 926 proteins. This resulted in a “plant-pathogen immune network, version 1” (PPIN-1) containing 3148 interactions (fig. S2 and table S2).

We display in Fig. 1, fig. S2, and an interactive Web interface (<http://signal.salk.edu/interactome/PPIN1.html>) PPIN-1 in four layers. (Fig. 1A shows the experimentally determined network, fig. S2, the derived PPIN-1.) The top layer contains effector proteins from both pathogens; the second layer consists of host proteins directly interacting

¹Department of Biology, University of North Carolina at Chapel Hill, Chapel Hill, NC 27599, USA. ²Center for Cancer Systems Biology (CCSB) and Department of Cancer Biology, Dana-Farber Cancer Institute, Boston, MA 02215, USA. ³Department of Genetics, Harvard Medical School, Boston, MA 02115, USA. ⁴Computational and Mathematical Biology Group, TIMC-IMAG, CNRS UMR5525 and Université de Grenoble, Faculté de Médecine, 38706 La Tronche cedex, France. ⁵Unité de Recherche en Biologie Moléculaire, Facultés Universitaires Notre-Dame de la Paix, 5000 Namur, Wallonia-Brussels Federation, Belgium. ⁶School of Life Sciences, University of Warwick, Wellesbourne, Warwick, CV35 9EF, UK. ⁷Warwick Systems Biology Centre, Coventry House, University of Warwick, Coventry, CV4 7AL, UK. ⁸Department of Biological Chemistry and Molecular Pharmacology, Harvard Medical School, Boston, MA 02115, USA. ⁹Genomic Analysis Laboratory, The Salk Institute for Biological Studies, La Jolla, CA 92037, USA. ¹⁰Biomedical Engineering Department, Boston University, Boston, MA 02215, USA. ¹¹Boston University School of Medicine, Boston, MA 02118, USA. ¹²Unité Mixte de Recherche en Génétique Végétale (URGV), UMR, Institut National de la Recherche Agronomique (INRA), Université d'Evry-Val d'Essonne—European Research Laboratory (UEVE-ERL), CNRS, 91057 Evry Cedex, France. ¹³Utrecht University, 3584 CH Utrecht, Netherlands. ¹⁴Department of Biological Chemistry and Molecular Pharmacology, Harvard Medical School, Boston, MA 02115, USA. ¹⁵Plant Biology Laboratory, Salk Institute for Biological Studies, La Jolla, CA 92037, USA. ¹⁶Curriculum in Genetics and Molecular Biology, University of North Carolina at Chapel Hill, Chapel Hill, NC 27599, USA. ¹⁷Carolina Center for Genome Science, University of North Carolina at Chapel Hill, Chapel Hill, NC 27599, USA. ¹⁸Department of Microbiology and Immunology, University of North Carolina at Chapel Hill, Chapel Hill, NC 27599, USA.

*These authors contributed equally to this project.

†Present address: Department of Biology, CH106, University of Alabama at Birmingham, 1300 University Boulevard, Birmingham, AL 35294, USA.

‡Present address: ADAS Boxworth Research Centre, Boxworth, Cambridgeshire CB23 4NN, UK.

§Present address: Max Planck Institute for Infection Biology, Charitéplatz 1, 10117 Berlin, Germany.

¶Present address: Donnelly Centre for Cellular and Biomolecular Research, University of Toronto, Toronto, Ontario M5S3E1, Canada, and Samuel Lunenfeld Research Institute, Mt. Sinai Hospital, Toronto, Ontario M5G1X5, Canada.

¶¶To whom correspondence should be addressed. E-mails: dangl@email.unc.edu (J.L.D.); pascal_braun@dfci.harvard.edu (P.B.); jim.beynon@warwick.ac.uk (J.B.); marc_vidal@dfci.harvard.edu (M.V.)

with those effectors (effector targets); the third layer depicts the three previously defined classes of *Arabidopsis* immune proteins: NB-LRR, defense proteins, and RLK proteins; and the fourth layer consists of immune interactors.

Of the 673 immune interactors, only 66 were among the 975 proteins encoded by open reading frames (ORFs) in AtORFeome2.0 with a Gene Ontology (GO) annotation related to immunity (GO-immune proteins) (table S3) ($P > 0.05$) (table S4). This may be because of the technical limitations of both large- and small-scale experiments (12–15) and limited knowledge about the plant immune system. Although 239 of the 673 immune interactors interacted with a GO-immune protein in the systematically mapped subset of AI-1, termed “AI-1_{MAIN}” [see Glossary (10) and (11)], 368 were neither GO-immune proteins nor previously known to interact with a GO-immune protein (fig. S3).

We identified 165 putative effector targets in PPIN-1, compared with ~20 described previously (16). Although the functions of most of these *Arabidopsis* proteins are unknown, they are enriched in GO annotations for regulation of transcription, metabolism, and nuclear localization (table S5) (10). We noted significant enrichment of the effector targets in immune- and hormone-related GO annotations (table S4) (10, 17). Angiosperm-specific proteins are over-represented among the effector targets, in comparison with all proteins encoded in AtORFeome2.0 ($P = 0.0007$) (table S4).

To characterize the transcriptional response of genes encoding proteins in PPIN-1, we categorized all corresponding proteins into 10 non-overlapping groups (table S6): two immune protein groups (the two combined classes of

receptors and the defense proteins); one group containing all effector proteins; and seven groups containing subsets of the immune interactors corresponding to their pattern of interactions with the three aforementioned groups (figs. S4 and S5 and table S7) (10). Many receptor genes were differentially regulated under a variety of defense-related conditions (fig. S5); however, genes encoding specific interactors of these receptors were not (figs. S4 and S5 and table S7). This suggests that pathogen detection sensitivity is specifically modulated via transcriptional regulation of receptor genes (18, 19). Receptors might also associate with proteins unrelated to the defense machinery.

PPIN-1 proteins evolve faster than those of AI-1. The LRR domains of both plant immune receptor classes exhibit footprints of positive diversifying selection (3, 20). Host-pathogen “arms races” are assumed to drive adaptive evolution of immune system genes, although this is an oversimplification for plant-pathogen interactions (21). We defined a set of 333 *Arabidopsis* genes with one-to-one orthology relations in Papaya (10) as a reference and estimated the ratio of nonsynonymous-to-synonymous mutations per site in their coding sequences (d_N/d_S) (Fig. 1B). Nonreceptor immune interactors are evolving very slowly overall, which suggests functional constraint and purifying selection. They nevertheless exhibit a significantly higher evolution rate than proteins in AI-1_{MAIN} ($P < 0.01$) (Fig. 1B) (10). This was not the case for control gene groups encoding hormone-related proteins (fig. S6A) (17) or metabolic enzymes (fig. S6B) (22, 23). Hence, even the nonreceptor proteins from PPIN-1 evolve faster than other protein groups or the proteins in AI-1_{MAIN} in general.

Pathogen effectors converge onto highly connected proteins in the plant interactome.

Our hypothesis was that many effectors from evolutionarily diverse pathogens would converge onto a limited set of defense-related host targets and molecular machines (4, 5), as opposed to each effector having evolved to target idiosyncratic, pathogen life-style-specific targets. To test this, we compared the number of effector targets identified in PPIN-1 to the number of targets expected with randomly assigned connections between effectors and *Arabidopsis* proteins (“random targets”). PPIN-1 defined 165 direct effector targets; 18 of these were targeted by effectors from both pathogens (Fig. 1A, and fig. S7A, left, and fig. S8, left) (10). In contrast, simulations identified an average of 320 random targets, of which less than 1% would be targeted by effectors from both pathogens ($P < 0.001$, empirical P value) (Fig. 2A and figs. S7A and S8) (10). We investigated the connectivity between the 137 observed effector targets that are also present in AI-1_{MAIN}. They are connected by 139 interactions in AI-1_{MAIN} ($P < 6.7 \times 10^{-5}$, empirical P value) (Fig. 2B and table S8), whereas we expect an average of only 22 (maximum 59) connections if effector targets were randomly distributed in a network with the same structure as AI-1_{MAIN} (Fig. 2B and fig. S7B). Collectively, these data support our hypothesis that diverse pathogens deploy virulence effectors that converge onto a limited set of host cellular machines.

Scale-free networks are resilient to random perturbations but sensitive and easily destabilized by targeted attack on their most highly connected hubs (24). AI-1_{MAIN} shares this property even though it is not perfectly scale-free (fig. S9). Simulations demonstrate that an attack on experimentally identified effector targets is much more damaging to the network structure than an attack on the same number of randomly selected proteins (fig. S9). Consistent with this, we found that the number of interaction partners (degree) of the effector targets present in AI-1_{MAIN} was significantly higher than that of proteins in AI-1_{MAIN} that are not in PPIN-1 (Fig. 2C). Remarkably, 7 of the 15 hubs of degrees greater than 50 (hubs₅₀) in AI-1_{MAIN} were targeted by effectors from both pathogens ($P = 6.5 \times 10^{-13}$) (tables S4 and S8), and 14 of the 15 hubs₅₀ were targeted by effectors from at least one pathogen ($P = 6.9 \times 10^{-18}$) (tables S4 and S8) (10), consistent with observations of human-virus infection systems (25–28).

We evaluated whether this connectivity explains the observed convergence (Fig. 2A and fig. S8). We performed simulations where the probability of an *Arabidopsis* protein to randomly interact with an effector was proportional to its degree in AI-1_{MAIN}. We found that 51 of 2661 AI-1_{MAIN} proteins were actually targeted significantly more often by effectors than expected given their respective degrees (e.g., “significant targets”) (table S8). These include 5 of the 14 hubs₅₀ that interact with effectors ($P = 5 \times 10^{-6}$) (Fig. 2D and table S4) and 4 of the 7 hubs₅₀ that are targeted by

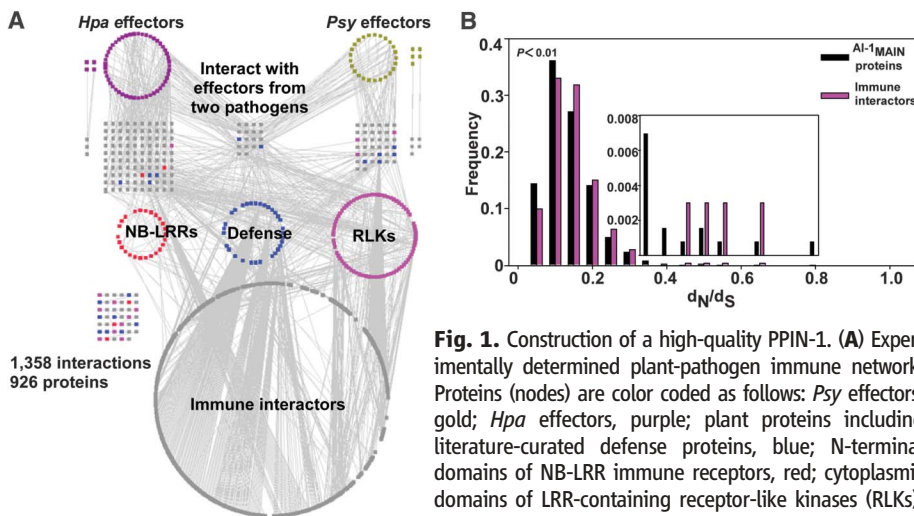


Fig. 1. Construction of a high-quality PPIN-1. (A) Experimentally determined plant-pathogen immune network. Proteins (nodes) are color coded as follows: *Psy* effectors, gold; *Hpa* effectors, purple; plant proteins including literature-curated defense proteins, blue; N-terminal domains of NB-LRR immune receptors, red; cytoplasmic domains of LRR-containing receptor-like kinases (RLKs), a subclass of pattern recognition receptors, pink; and immune interactors, gray. Gray edges represent protein-protein interactions. Interactions that are not connected to the network involving *Hpa* or *Psy* effectors are indicated next to their relevant protein categories in the first and second layers. Grid at left denotes individual interactions involving immune proteins. (B) PPIN-1 proteins evolve faster than those of AI-1. Distribution of d_N/d_S ratios computed between *Arabidopsis* proteins and their Papaya orthologs for all AI-1_{MAIN} proteins and for immune interactors [from (A)] present in AI-1_{MAIN}. Inset is rescaled on the y axis to make the higher d_N/d_S categories more apparent. The x axis remains the same for the inset. P value from Kolmogorov-Smirnov test.

immune interactors, gray. Gray edges represent protein-protein interactions. Interactions that are not connected to the network involving *Hpa* or *Psy* effectors are indicated next to their relevant protein categories in the first and second layers. Grid at left denotes individual interactions involving immune proteins. (B) PPIN-1 proteins evolve faster than those of AI-1. Distribution of d_N/d_S ratios computed between *Arabidopsis* proteins and their Papaya orthologs for all AI-1_{MAIN} proteins and for immune interactors [from (A)] present in AI-1_{MAIN}. Inset is rescaled on the y axis to make the higher d_N/d_S categories more apparent. The x axis remains the same for the inset. P value from Kolmogorov-Smirnov test.

effectors from both pathogen species ($P = 0.006$) (table S4). Among the 17 proteins interacting with effectors from both pathogens that are also present in AI-1_{MAIN}, 12 are significant targets ($P = 0.003$) (table S4). These results indicate that the convergence of effectors onto a set of host targets cannot be explained merely by the high connectivity of those targets and, thus, likely reflects additional aspects of the host-pathogen co-evolution history.

In addition to effector targets, other PPIN-1 proteins displayed high connectivity in AI-1_{MAIN} (Fig. 2, C and E). Consequently, immune interactors form a highly connected cluster in the plant interactome (figs. S10 and S11A). This is not the case for well-annotated subnetworks involved in hormone-related or metabolic processes (fig. S11, B and C) (17, 22, 23). Thus, PPIN-1 proteins as a whole, and effector targets in particular, are highly connected nodes within the overall plant network.

The plant response: Guarding high-value targets. We found that only 2 out of 30 NB-LRR immune receptor fragments in PPIN-1 directly interacted with a pathogen effector ($P = 0.04$) (table S4). In contrast, nearly half of the NB-LRR interactors (24 out of 52), including 7 of the 15 hubs₅₀, were effector targets ($P = 4.6 \times 10^{-5}$ and $P = 8 \times 10^{-12}$, respectively) (table S4). N-terminal domains of NB-LRRs can associate with either cellular targets of effector action or with downstream signaling components (10). Thus, our results are consistent with the proposition that NB-LRR proteins can monitor the integrity of cellular proteins and are activated when pathogen effectors act to generate “modified self” molecules (4, 5) for the 30 NB-LRR proteins fragments present in PPIN-1. We note that the interactors of full-length NB-LRR proteins in AI-1_{MAIN} include two of the hub₅₀ proteins that are targeted by both pathogens (TCP14 and CSN5a) (11). Furthermore, in PPIN-1 only 4 of 90 putative RLK receptors interacted directly with a pathogen effector ($P = 10^{-5}$) (table S4), whereas 46 of 162 interactors of RLKs were effector targets ($P = 0.02$) (table S4). This contrasts with the direct perturbation of PRR-RLK kinase function observed for two *Psy* type III effectors (2). In sum, our observations are consistent with the view that pathogen effectors are mostly indirectly connected to at least those host immune receptors represented in PPIN-1.

Effector targets and immune receptors participate in diverse potential protein modules. Many effector targets are cellular hubs and, thus, likely to be part of various protein modules across different cellular and developmental contexts. We extracted modules of two, three, or four physically connected PPIN-1 proteins (Fig. 3 and table S9) and found that the 18 proteins targeted by effectors from both pathogens were involved in 303 combinatorial modules of *Psy* effector–*Arabidopsis* protein–*Hpa* effector (Fig. 3, A and B). Similarly, we noted several hundred combinatorial modules involving 192 interacting *Arabidopsis* protein pairs where both partners are targeted by effectors from one or both pathogens (Fig. 3, A and B, and table

S9). Of the 105 effector targets involved in these modules, 91 are present in AI-1_{MAIN}, where they have an average degree of 29 (compared with an

average degree of 4.8 and 2.6 for PPIN-1 and non-PPIN-1 proteins, respectively, in AI-1_{MAIN}). The targeting of an *Arabidopsis* protein, or a pair

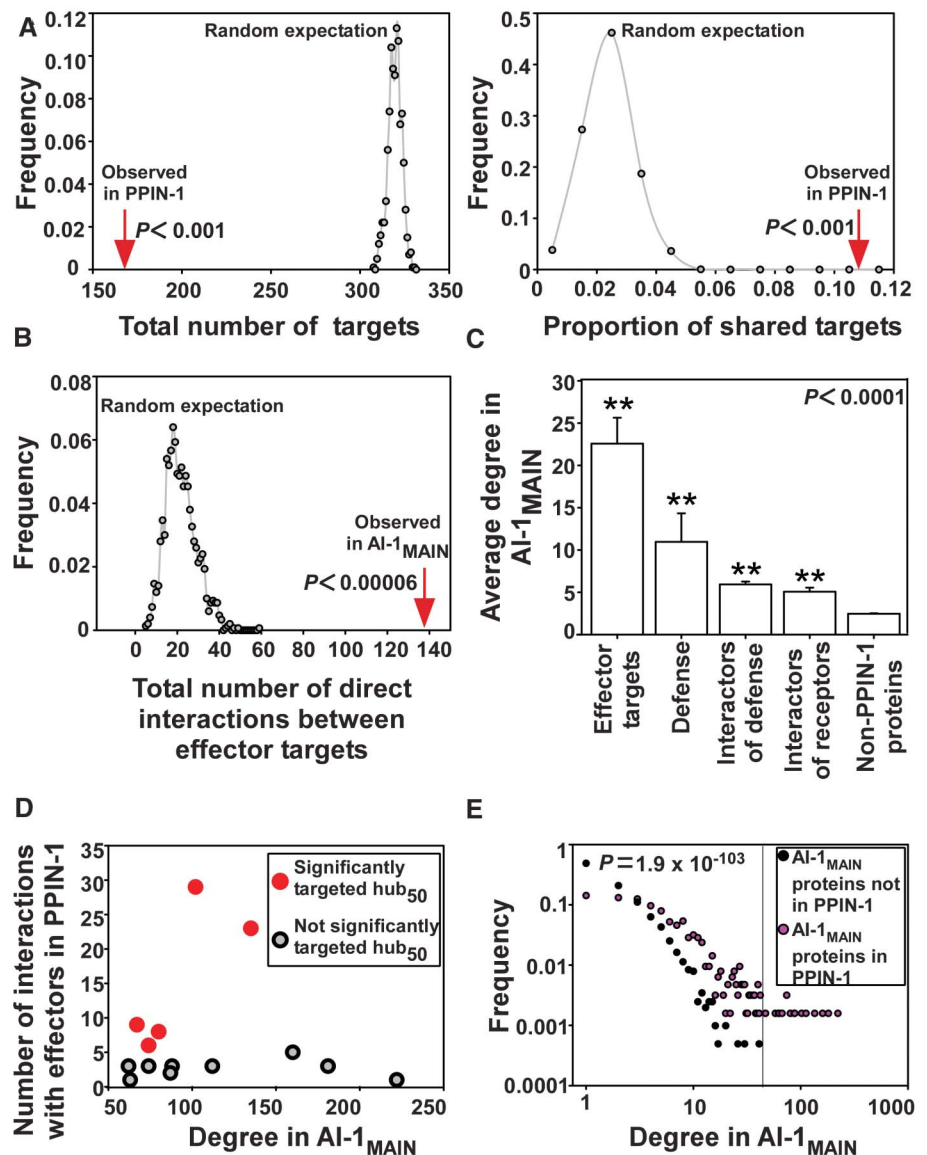


Fig. 2. Effector proteins converge onto interconnected cellular hubs. (A) Significance of the convergence of effectors onto a limited set of targets. Distribution of the total number of effector targets (left) and of the proportion of shared targets (right) in 1000 simulations (10). The red arrows represent the observed number of effector targets in PPIN-1 (left) (Figs. 1A and 3A and figs. S7 and S8) and the observed proportion of shared targets in PPIN-1 (right) (Figs. 1A and 3A and figs. S7 and S8). (B) Significance of the connectivity among effector targets. Distribution of the number of direct connections between effector targets in 15,000 simulations (10). The red arrows represent the observed number of interactions between effector targets in AI-1_{MAIN}. (C) PPIN-1 proteins display a high connectivity in AI-1_{MAIN}. The average degree (number of interactors) in AI-1_{MAIN} of PPIN-1 proteins groups (Fig. 1A) was compared with proteins in AI-1_{MAIN} that are not in PPIN-1. All groups of proteins from PPIN-1 have a significantly higher degree than non-PPIN-1 proteins in AI-1_{MAIN} ($**P < 0.0001$, Mann-Whitney *U* test). Receptors include both NB-LRRs and RLKs. Error bars, standard error of the mean. (D) Five hubs₅₀ are targeted by significantly more effectors than expected given their degree in AI-1_{MAIN}. Each dot represents a hub₅₀ targeted by at least one effector in PPIN-1, graphed as a function of both its degree in AI-1_{MAIN} (x axis) and of the number of interactions it has with effectors in PPIN-1 (y axis). Dots colored red correspond to hubs₅₀ that are targeted by significantly more effectors than expected given their degree ($P < 0.05$, empirical *P* value from degree-preserving random simulations) (10). (E) Relative frequency of degree in AI-1_{MAIN} of (i) the 632 PPIN-1 proteins present in AI-1_{MAIN} (pink) and (ii) the remaining 2029 proteins in AI-1_{MAIN} (black). Group (i) shows a significantly higher degree distribution than group (ii) according to a Mann-Whitney *U* test ($P = 1.9 \times 10^{-103}$). The vertical line corresponds to a degree of 50.

of interacting proteins, by effectors from both pathogens suggests an important function for these cellular machines. We do not infer that these combinations exist *in vivo*, because both pathogens rarely infect the same plant. We also found 19 and 41 proteins interacting with only *Psy* or *Hpa* effectors, respectively (Fig. 3, A and B); this apparent pathogen specificity may reflect the limited sensitivity of our experimental pipeline (11) or pathogen life-style-specific interactions. We also assembled a number of combinatorial modules where pathogen effectors indirectly interacted with either an RLK (855) or NB-LRR (249) receptor domain protein via an *Arabidopsis* protein (Fig. 3C). Furthermore, single *Arabidopsis* proteins mediated combinatorial modules between a cytoplasmic RLK domain and an NB-LRR N terminus in 119 cases (Fig. 3C).

Experimental validation of host proteins targeted by multiple pathogen effectors. We functionally validated the 18 proteins targeted by effectors from both pathogens (Figs. 1A and 3A). This subset includes 7 of the 15 hubs₅₀ proteins from AI-1_{MAIN} (table S8). We assayed whether

these effector targets function to positively regulate host defense (mutation leads to enhanced host susceptibility), negatively regulate host defense (mutation leads to enhanced host resistance), or function to facilitate infection (mutation also leads to enhanced host resistance). We discovered enhanced disease susceptibility to two different *Hpa* isolates, Emwa1 and Emoy2, for 9 of 17 loci for which insertion mutants were available (29, 30) (Fig. 4A, fig. S12A, and table S10). Mutants in the eight remaining loci did not exhibit enhanced disease susceptibility. However, at least six of these eight exhibited enhanced disease resistance to the virulent *Hpa* isolate Noco2 (Fig. 4B and table S10). Moreover, this enhanced disease-resistance phenotype was maintained at a later time point in the infection cycle (table S10). Hence, 15 of 17 proteins targeted by effectors from both pathogens, including all 7 of the 15 hubs₅₀ proteins, have mutant phenotypes, consistent with immune system functions. Preliminary observations also suggest that the mutants for JAZ3 (At3g17860) and LSU2 (At5g24660) expressed an enhanced disease

susceptibility phenotype after inoculation with *P. syringae* DC3000(*avrRpt2*) (fig. S12B), in addition to being required for full immune function during *Hpa* infection (Fig. 4A). This suggests that these genes are required for pathogen growth-suppression mediated by the resistance to *P. syringae* 2 (RPS2) NB-LRR protein.

In yeast, deletion of genes encoding hubs in a binary protein interaction network tend to cause multiple phenotypes (15). We were therefore surprised that the seven hubs₅₀ among the 17 proteins targeted by effectors from both pathogens did not express pleiotropic morphological mutant phenotypes. CSN5a (At1g22920), a subunit of the COP9 signalosome and a hub₅₀ in AI-1_{MAIN}, did. CSN5a interacts with 29 distinct effectors from *Hpa* and *Psy* in our experiment and is a demonstrated target of a geminiviral virulence protein (31). It also interacts with the N termini of NB-LRR proteins and the cytoplasmic domains of RLKs (table S9). The morphological consequences of *csn5a* pleiotropy can be suppressed by reducing the expression of either of the two *Arabidopsis* CUL3 subunits (32). We found that *csn5a-2 cul3a*

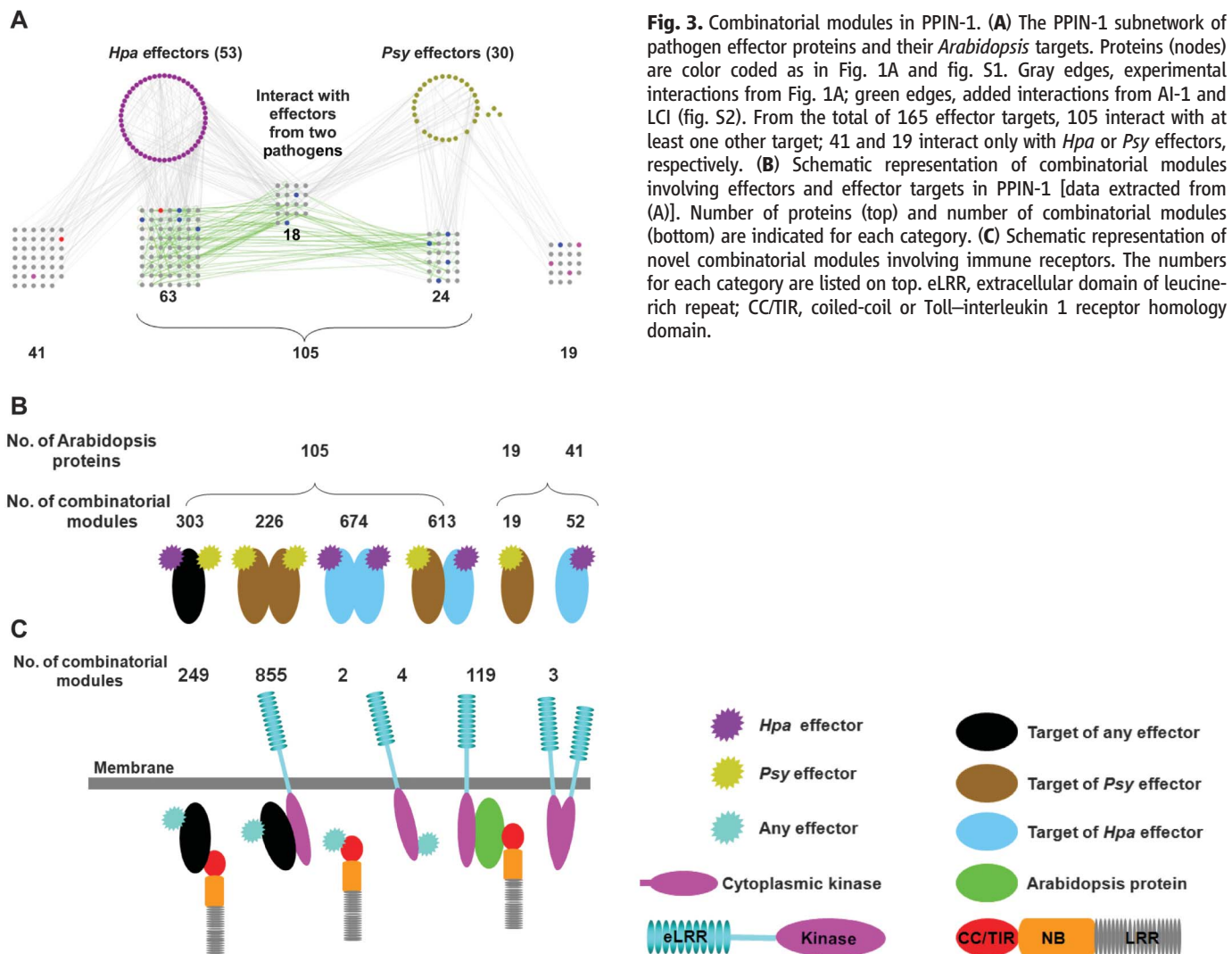


Fig. 3. Combinatorial modules in PPIN-1. **(A)** The PPIN-1 subnetwork of pathogen effector proteins and their *Arabidopsis* targets. Proteins (nodes) are color coded as in Fig. 1A and fig. S1. Gray edges, experimental interactions from Fig. 1A; green edges, added interactions from AI-1 and LCI (fig. S2). From the total of 165 effector targets, 105 interact with at least one other target; 41 and 19 interact only with *Hpa* or *Psy* effectors, respectively. **(B)** Schematic representation of combinatorial modules involving effectors and effector targets in PPIN-1 [data extracted from (A)]. Number of proteins (top) and number of combinatorial modules (bottom) are indicated for each category. **(C)** Schematic representation of novel combinatorial modules involving immune receptors. The numbers for each category are listed on top. eLRR, extracellular domain of leucine-rich repeat; CC/TIR, coiled-coil or Toll–interleukin 1 receptor homology domain.

seedlings displayed enhanced disease resistance compared with controls after infection with virulent *Hpa* (Fig. 4C). These results correlated with infection-triggered overaccumulation of PR1 protein, a common marker for MTI, in *Hpa*- (fig. S12C) or *Psy*-infected (fig. S12D) *csn5a-2 cul3a* plants, compared with Col-0. Hence, our observed enhanced disease-resistance phenotype of *csn5a* is not due to its pleiotropic morphological phe-

notypes. Many proteins are substrates for CSN5a-dependent degradation, perhaps including many of its interactors; thus, its elimination or perturbation by effectors could plausibly alter immune function by altering clearance of both host and pathogen proteins.

We also validated prefoldin 6 (PFD6; At1g29990) (Fig. 4D and fig. S13) because of its interaction with the known defense regulator EDS1 (enhanced

disease susceptibility 1) and two bacterial effectors (table S9) (10). We tested whether *pfd6-1* exhibited signs of modified MTI by assaying flagellin (flg22 peptide)-induced disease resistance. Bacterial growth in flg22 pretreated leaves of Col-0 plants was 1/10th to 1/20th that in mock pretreated leaves, which reflected successful MTI. This flg22-induced MTI was compromised in *pfd6-1* plants (Fig. 4D). Transcriptional induction of

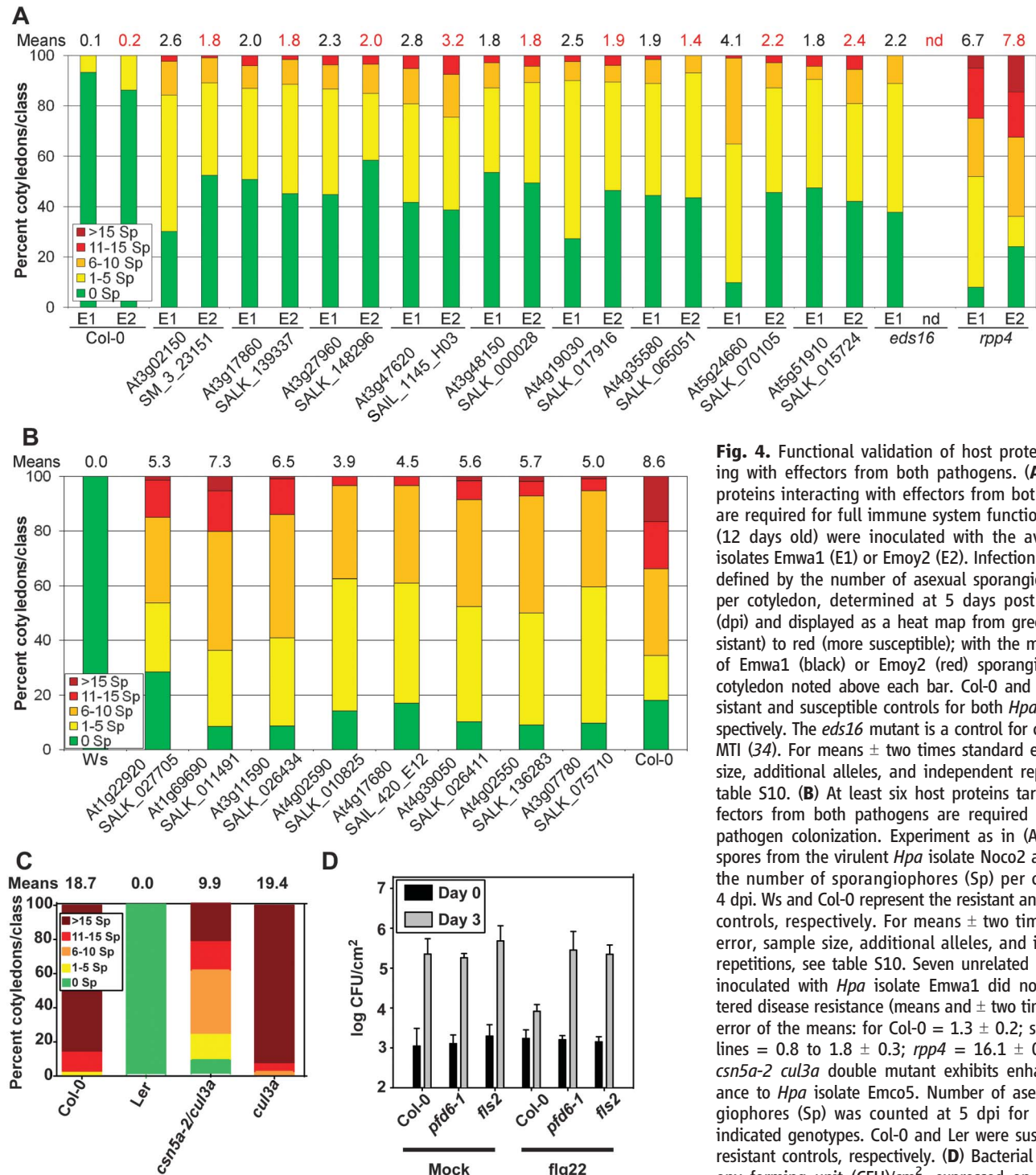


Fig. 4. Functional validation of host proteins interacting with effectors from both pathogens. **(A)** Nine host proteins interacting with effectors from both pathogens are required for full immune system function. Seedlings (12 days old) were inoculated with the avirulent *Hpa* isolates Emwa1 (E1) or Emoy2 (E2). Infection classes were defined by the number of asexual sporangiophores (Sp) per cotyledon, determined at 5 days post inoculation (dpi) and displayed as a heat map from green (more resistant) to red (more susceptible); with the mean number of Emwa1 (black) or Emoy2 (red) sporangiophores per cotyledon noted above each bar. Col-0 and *rpp4* are resistant and susceptible controls for both *Hpa* isolates, respectively. The *eds16* mutant is a control for compromised MTI (34). For means \pm two times standard error, sample size, additional alleles, and independent repetitions see table S10. **(B)** At least six host proteins targeted by effectors from both pathogens are required for maximal pathogen colonization. Experiment as in (A), but using spores from the virulent *Hpa* isolate Noco2 and counting the number of sporangiophores (Sp) per cotyledon at 4 dpi. Ws and Col-0 represent the resistant and susceptible controls, respectively. For means \pm two times standard error, sample size, additional alleles, and independent repetitions, see table S10. Seven unrelated mutant lines inoculated with *Hpa* isolate Emwa1 did not exhibit altered disease resistance (means and \pm two times standard error of the means: for Col-0 = 1.3 ± 0.2 ; seven mutant lines = 0.8 to 1.8 ± 0.3 ; *rpp4* = 16.1 ± 0.7). **(C)** The *csn5a-2 cul3a* double mutant exhibits enhanced resistance to *Hpa* isolate Emco5. Number of asexual sporangiophores (Sp) was counted at 5 dpi for each of the indicated genotypes. Col-0 and Ler were susceptible and resistant controls, respectively. **(D)** Bacterial growth [colony forming unit (CFU)/cm², expressed on a log scale]

after flg22 (right) or mock treatment (water, left) of leaves of the indicated genotypes followed 24 hours later by infection with *Pto* DC3000. Bacterial growth was assessed at 3 dpi. Error bars, two standard errors of the mean ($n = 4$).

molecular MTI markers was abolished in the *fls2* mutant, which lacks the PRR receptor for flg22 peptide, and largely impaired in *pdf6-1* (fig. S13). These results link PFD6 to MTI downstream of FLS2 PRR receptor function (10, 33). Collectively, these results (Fig. 4) validate the biological significance of PPIN-1 and confirm that pathogen effectors target host proteins that are required for effective defense or pathogen fitness. To facilitate further hypothesis testing, we present the local networks for the five significantly targeted hubs (Fig. 2D and table S4) and point out connections to cellular functions potentially relevant to immune system function (figs. S14 to S18).

Conclusions. Our analyses reveal that oomycete and bacterial effectors separated by ~2 billion years of evolution target an overlapping subset of plant proteins that include well-connected cellular hubs. Our functional validation supports the notion that effectors are likely to converge onto interconnected host machinery to suppress effective host defense and to facilitate pathogen fitness. We predict that many of the 165 effector targets we defined will also be targets of additional, independently evolved effectors from other plant pathogens. We anticipate that effectors that target highly connected cellular proteins fine-tune cellular networks to increase pathogen fitness and that evolutionary forces integrate appropriate immune responses with those perturbations. As proposed in the guard hypothesis, our data are consistent with indirect connections between pathogen effectors and NB-LRR immune receptors, at least for the NB-LRR fragments represented in PPIN-1. The high degree of the effector targets argues against a decoy role for these proteins. Although the concept of cellular decoys evolved to intercept pathogen effectors is attractive, and likely true in one case in the plant immune system (3), these are expected to have few, if any, additional cellular functions and, as such, would likely have fewer interaction partners in the protein interaction network. Most of the 673 immune interactors have no previously described immune-system function. Our results bridge plant immunology, which predicted that effectors should target common proteins, and network science, which proposes that hubs should be targets for network manipulation (25–28). Derivation of general rules regarding the organization and function of host cellular machinery required for effective defense against microbial infection, as well as detailed mechanistic understanding of how pathogen effectors manipulate these machines to increase their fitness, will facilitate improvement of plant immune system function.

References and Notes

1. C. Zipfel, *Curr. Opin. Plant Biol.* **12**, 414 (2009).
2. T. Boller, S. Y. He, *Science* **324**, 742 (2009).
3. P. N. Dodds, J. P. Rathjen, *Nat. Rev. Genet.* **11**, 539 (2010).
4. J. L. Dangl, J. D. Jones, *Nature* **411**, 826 (2001).
5. J. D. Jones, J. L. Dangl, *Nature* **444**, 323 (2006).
6. E. Lukasik, F. L. Takken, *Curr. Opin. Plant Biol.* **12**, 427 (2009).
7. G. van Ooijen *et al.*, *J. Exp. Bot.* **59**, 1383 (2008).
8. D. A. Baltus *et al.*, *PLoS Pathog.* **7**, e1002132 (2011).
9. L. Baxter *et al.*, *Science* **330**, 1549 (2010).

10. Glossary, materials and methods, supporting figures, and supporting tables are available as supporting material on *Science Online*.
11. Arabidopsis Interactome Mapping Consortium, *Science* **333**, 601 (2011).
12. M. Dreze *et al.*, *Methods Enzymol.* **470**, 281 (2010).
13. P. Braun *et al.*, *Nat. Methods* **6**, 91 (2009).
14. M. E. Cusick *et al.*, *Nat. Methods* **6**, 39 (2009).
15. H. Yu *et al.*, *Science* **322**, 104 (2008).
16. J. D. Lewis, D. S. Guttman, D. Desveaux, *Semin. Cell Dev. Biol.* **20**, 1055 (2009).
17. Z. Y. Peng *et al.*, *Nucleic Acids Res.* **37**, (Database issue), D975 (2009).
18. X. Tan *et al.*, *BMC Plant Biol.* **7**, 56 (2007).
19. C. Zipfel *et al.*, *Nature* **428**, 764 (2004).
20. T. B. Sackton *et al.*, *Nat. Genet.* **39**, 1461 (2007).
21. E. B. Holub, *Nat. Rev. Genet.* **2**, 516 (2001).
22. P. Zhang *et al.*, *Plant Physiol.* **138**, 27 (2005).
23. Y. Jaillais, J. Chory, *Nat. Struct. Mol. Biol.* **17**, 642 (2010).
24. R. Albert, H. Jeong, A. L. Barabasi, *Nature* **406**, 378 (2000).
25. B. de Chasse *et al.*, *Mol. Syst. Biol.* **4**, 230 (2008).
26. M. D. Dyer *et al.*, *PLoS ONE* **5**, e12089 (2010).
27. M. A. Calderwood *et al.*, *Proc. Natl. Acad. Sci. U.S.A.* **104**, 7606 (2007).
28. P. Uetz *et al.*, *Science* **311**, 239 (2006).
29. J. M. Alonso *et al.*, *Science* **301**, 653 (2003).
30. A. Sessions *et al.*, *Plant Cell* **14**, 2985 (2002).
31. R. Lozano-Durán *et al.*, *Plant Cell* **23**, 1014 (2011).
32. G. Gusmaroli, P. Figueroa, G. Serino, X. W. Deng, *Plant Cell* **19**, 564 (2007).
33. S. Robertzek, D. Chinchilla, T. Boller, *Genes Dev.* **20**, 537 (2006).
34. K. Tsuda, M. Sato, J. Glazebrook, J. D. Cohen, F. Katagiri, *Plant J.* **53**, 763 (2008).

Acknowledgments: This work was funded by NIH GM-066025, NSF 2010 0929410, and U.S. Department of Energy (DOE) FG02-95ER20187 to J.L.D.; U.K. Biotechnology and Biological Sciences Research Council E024815, F005806 and G015066 to J.B.; NSF 0703905

to M.V., J.R.E., D.E.H.; NIH P50-HG004233 to M.V.; and NSF 0520253, 0313578 and 0726408 to J.R.E. D.M. was supported by AGRONOMIC LSNG-CT-2006-037704 from Sixth Framework Programme of the European Commission to C. Lurin. We acknowledge that the NSF funded the *Arabidopsis* Biological Research Center and the Salk Institute Genomic Analysis Laboratory (SIGnAL) projects for seeds and clones, respectively. We thank L. Baxter (Warwick Systems Biology, UK) for *Arabidopsis*/Papaya ortholog identification; B. Charlotiaux (Center of Cancer Systems Biology, Boston, USA) for assisting in some bioinformatics analyses; B. Kemmerling (University of Tuebingen, Germany) for several RLK clones not contained in SIGnAL; and C. Somerville and Y. Gu (University of California, Berkeley, USA), T. Mengiste (Purdue University, USA), and X.-W. Deng (Yale University, USA) for seeds. The EU Effectomics Consortium was funded by the European Research Area in Plant Genomics and includes A. Cabral and G. van den Ackerveken (Utrecht University, The Netherlands); J. Bator, R. Yatusевич, S. Katou and J. Parker (Max Planck Institute for Plant Breeding Research, Cologne, Germany); G. Fabro and J. Jones (The Sainsbury Laboratory, Norwich, UK); and M. Coates and T. Payne (University of Warwick, Warwick, UK). M.V. is a Chercheur Qualifié Honoraire from the Fonds de la Recherche Scientifique (FRS-FNRS, Wallonia-Brussels Federation, Belgium). Binary interaction data are supplied in table S2 in SOM. Homozygous mutant seed stocks noted in Figure 4 are available from the Arabidopsis Biological Resource Center (ABRC). Author contributions are listed in the SOM.

Supporting Online Material

www.sciencemag.org/cgi/content/full/333/6042/596/DC1
Materials and Methods
SOM Text
Figs. S1 to S18
Tables S1 to S10
References

1 February 2011; accepted 6 June 2011
10.1126/science.1203659

Evidence for Network Evolution in an *Arabidopsis* Interactome Map

Arabidopsis Interactome Mapping Consortium*†

Plants have unique features that evolved in response to their environments and ecosystems. A full account of the complex cellular networks that underlie plant-specific functions is still missing. We describe a proteome-wide binary protein-protein interaction map for the interactome network of the plant *Arabidopsis thaliana* containing about 6200 highly reliable interactions between about 2700 proteins. A global organization of plant biological processes emerges from community analyses of the resulting network, together with large numbers of novel hypothetical functional links between proteins and pathways. We observe a dynamic rewiring of interactions following gene duplication events, providing evidence for a model of evolution acting upon interactome networks. This and future plant interactome maps should facilitate systems approaches to better understand plant biology and improve crops.

Classical genetic and molecular approaches have provided fundamental understanding of processes such as growth control or development and molecular descriptions of genotype-to-phenotype relationships for a variety

of plant systems. Yet, more than 60% of the protein-coding genes of the model plant *Arabidopsis thaliana* (hereafter *Arabidopsis*) remain functionally uncharacterized. Knowledge about the biological organization of macromolecules in complex and dynamic “interactome” networks is lacking for *Arabidopsis* (fig. S1 and tables S1 and S2), depriving us of an understanding of how genotype-to-phenotype relationships are mediated at the systems level (1).

*All authors with their affiliations and contributions are listed at the end of the paper.

†To whom correspondence should be addressed. E-mail: marc_vidal@dfci.harvard.edu; ecker@salk.edu; pascal_braun@dfci.harvard.edu; david_hill@dfci.harvard.edu